



Cite this: RSC Adv., 2017, 7, 55282

Received 23rd September 2017
Accepted 30th November 2017DOI: 10.1039/c7ra10546k
rsc.li/rsc-advances

Electronic and photocatalytic properties of N/F co-doped anatase TiO_2 [†]

Yafei Zhao,  ^a Wei Wang, ^a Can Li^b and Liang He^{*a}

The crystal structure, formation energies, electronic structures and effective masses of charge carriers of N/F co-doped anatase TiO_2 were investigated by first principle calculations. We have found that the incorporation of the N atom will be easier in the presence of the F dopant. Second, the impurity band of N/F co-doped TiO_2 has no spin polarization and smaller effective mass, which improves the photogenerated carriers' mobility and separation. Moreover, it has a lower band edge energy, which increases the oxidation ability of the photogenerated holes. Thus, we explained the mechanism of the enhancement of photocatalytic efficiency of N/F co-doped TiO_2 observed from experiments.

1. Introduction

TiO_2 has attracted much interest and been widely utilized in photoelectrochemical devices, photovoltaic solar cells and the atmospheric environment, because of its low cost, nontoxicity, chemical inertness, oxidizing potential and high photocatalytic activity.^{1–4} However, practical applications of TiO_2 have been restricted by its large intrinsic band gap. Thus, it can only be excited by ultra-violet (UV) light (about 5% of the solar spectrum).^{5–7}

Doping nonmetal or metal elements is considered to be a promising method to reduce the absorption threshold of semiconductor-based photocatalysts (TiO_2 , ZnO *etc.*) and to move it from UV to visible light (about 45% of the solar spectrum).^{8–12} However, it is generally found that single element doped TiO_2 has limited visible light photocatalytic performance.^{13–18} Such as, although much work has suggested that N doping of TiO_2 extends the optical absorption edge into the visible light region, increased photocatalytic efficiency is still limited.^{15,19} On the other hand, co-doping two elements in TiO_2 demonstrates remarkable enhancement of photocurrent and photocatalyst effect, such as B and N co-doping,²⁰ C and N co-doping,^{21,22} C and F co-doping,²³ N and S co-doping,^{24,25} and N and F co-doping.^{26–30} Among them, N and F co-doping are particular interesting, because the formation of the impurity levels (ILs) effectively lowering the bulk band, and charge compensation effect between N and F atoms reducing the recombination rate of photogenerated electron–hole pairs.⁹

However, there is almost no relevant theoretical study performed on the influence of photogenerated carrier effective mass and ORR over the enhanced photocatalytic efficiency of the N/F co-doped TiO_2 . Thus, a systematically first principles study was conducted on the crystal structures, formation energy, electronic structures and effective masses of charge carriers. The results show that the Ti-rich growth condition is favorable to all doped TiO_2 ; meanwhile, the incorporation of the N atom into the TiO_2 will be promoted in the presence of the F dopant. Moreover, N/F co-doped TiO_2 not only greatly improves the photogenerated carriers' mobility and separation, but also increases the oxidation ability of the photogenerated holes; especially $\text{N}_s\text{--F}_s$ co-doped TiO_2 . This explains why $\cdot\text{OH}$ radical dominates the process of photocatalytic degradation of methylene blue.

2. Computational methods

First-principle density functional theory (DFT) calculations are performed using the CASTEP code. Norm-conserving pseudopotentials and Perdew–Burke–Ernzerhof for Solids (PBESOL) function of the generalized gradient approximation (GGA) are used for the electron–ion interactions and exchange–correlation potential, respectively.^{31,32} All simulations are carried out for a $2 \times 2 \times 1$ supercell with 16 Ti atoms and 32 O atoms. In the N-doped system, we only consider the N atom substitutes the O atom (N_s), which is consistent with the previous experimental results.^{15,26} For co-doped TiO_2 model, N atom and F atom are simultaneously introduced into the supercell of TiO_2 , they substitutes the O atom (N_s or F_s) or occupy the interstitial position (N_i or F_i). This is resulted in four different kinds of N/F co-doped TiO_2 , namely, $\text{N}_s\text{--F}_s$, $\text{N}_s\text{--F}_i$, $\text{N}_i\text{--F}_s$ and $\text{N}_i\text{--F}_i$ co-doped TiO_2 . In addition, we have considered the physical doping position of N and F atoms, and calculated the total energies of all possible configurations (based on the doped distance between N and F), as shown in ESI Fig. S1.[†] Only the most stable

^aNational Laboratory of Solid State Microstructures, School of Electronic Science and Engineering, Collaborative Innovation Center of Advanced Microstructures, Nanjing University, Nanjing 210093, China. E-mail: heliang@nju.edu.cn

^bCenter for Coordination Bond Engineering, College of Materials Science and Engineering, China Jiliang University, Hangzhou 310018, China

[†] Electronic supplementary information (ESI) available. See DOI: [10.1039/c7ra10546k](https://doi.org/10.1039/c7ra10546k)



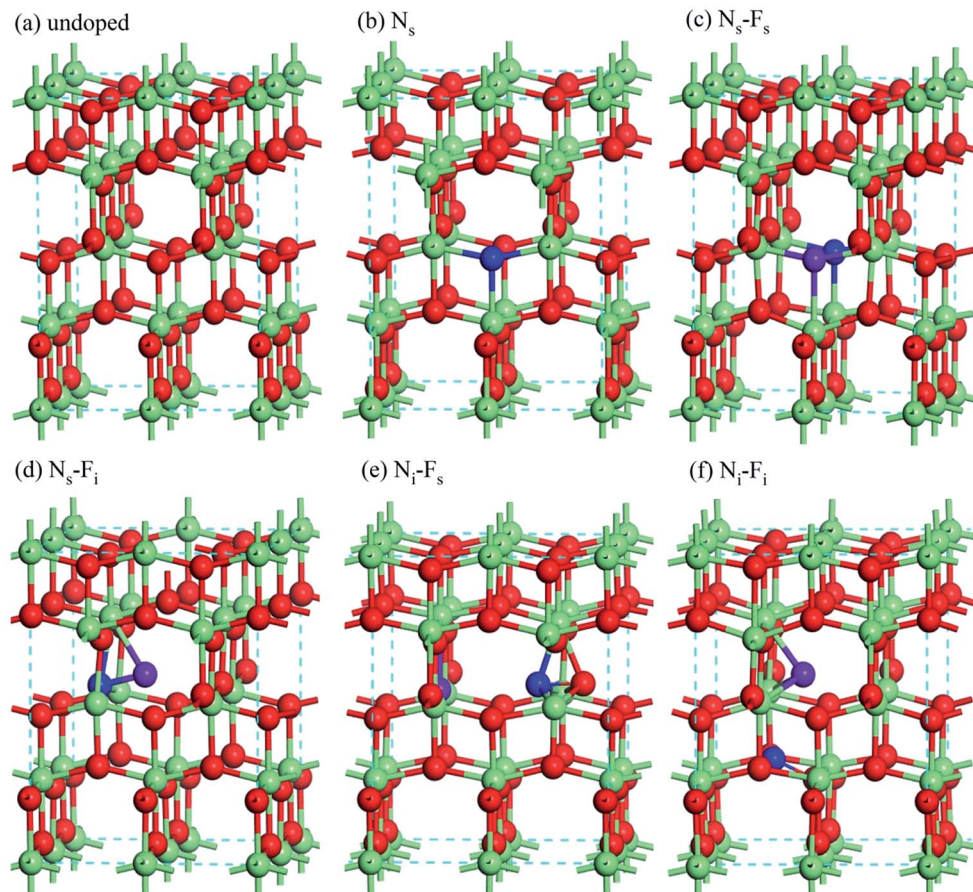


Fig. 1 The crystal structures of undoped and doped TiO_2 , where green, red, blue and purple balls are the Ti, O, N and F atoms, respectively.

configurations for each case of doped TiO_2 are shown in Fig. 1. The doping concentration (atom ratio) of the N or F ranges is chosen as around 2.08%, similar to the concentration used in the experiments.^{26,29,33,34}

The cutoff energy with 750 eV and $4 \times 4 \times 3$ k -point sampling set are sufficiently large for the systems considered. The convergence tolerance of energy, maximum displacement, and maximum force are 5.0×10^{-6} eV per atom, 5.0×10^{-4} Å, and 0.01 eV Å⁻¹, respectively. On the other hand, DFT calculations underestimate the band gap, and DFT+ U , as the improvement of standard DFT can overcome this situation. In this work, U values were selected 7.0 eV for Ti elements based on the calculated band-gap for anatase TiO_2 as a function of the U parameter in our previous work.³⁵ And, the energy for the band gap (E_g) of undoped anatase TiO_2 is 3.05 eV, which is consisted with the experimental value (3.20 eV) and other DFT+ U and HSE06 calculated values.^{36,37}

We calculated the E_f to assess the stability of all the doped systems:

$$E_s = E_{\text{doped}} - E_{\text{undoped}} - m\mu_N - n\mu_F + x\mu_O \quad (1)$$

where E_{doped} and E_{undoped} are the total energies of doped and undoped TiO_2 . The m and n denotes the number of N and F atoms doped into the supercell of TiO_2 , respectively. The x represents the numbers of O atoms substituted by dopants

atoms. In view of the growth of TiO_2 being a dynamic process, the formation energy is unfixed and depends on the growth condition (changing from O-rich condition to Ti-rich condition). Relations between μ_O and μ_N , μ_F , μ_{Ti} are satisfying the equations:

$$\mu_{\text{Ti}} + 2\mu_O = \mu(\text{TiO}_2) \quad (2)$$

$$\mu_N + 2\mu_O = \mu(\text{NO}_2) \quad (3)$$

$$3\mu_F + \mu_O = \mu(\text{OF}_3) \quad (4)$$

Under O-rich condition, μ_O is the chemical potential of the ground-state of the O_2 molecule; μ_{Ti} , μ_N and μ_F are obtained by the eqn (2), (3) and (4), respectively. Under Ti-rich condition, the μ_{Ti} is the chemical potential of Ti bulk, while μ_O , μ_N and μ_F are calculated by the eqn (2), (3) and (4), respectively. The simulation bond lengths of the O_2 , NO_2 and OF_3 molecules are close to the experimental value.³⁸

3. Result and discussion

3.1 Crystal structure and formation energies

Table 1 lists the calculated lattice constants of the undoped and doped TiO_2 . The lattice constants of undoped TiO_2 is consistent with the previous experimental results.³⁹ Overall, the effect of



Table 1 The equilibrium supercell lattice constants a , b and c with unit Å. V is the volume of all systems with unit Å³. E_f (Ti-rich and O-rich) E_F , E_g , E_{\max} , E_{CBM} and E_{VBM} are the calculated formation energy, Fermi level, band gap, the maximum energy gap in the band gap, the energy of CBM and VBM, respectively, with unit eV. m^* is the carrier effective mass compared with electronic mass

System	TiO ₂	N _s	N _s –F _s	N _s –F _i	N _i –F _s	N _i –F _i
<i>a</i>	7.551	7.587	7.564	7.573	7.565	7.602
<i>b</i>	7.551	7.543	7.607	7.554	7.595	7.550
<i>c</i>	9.627	9.615	9.589	9.696	9.655	9.695
<i>V</i>	548.91	550.25	551.74	554.67	554.74	556.45
E_f	Ti-rich	—	–1.79	–6.92	–3.73	–4.77
	O-rich	—	5.77	4.01	4.68	3.63
E_F		6.41	4.08	4.09	3.65	4.10
E_{CBM}		9.46	7.06	6.47	6.70	6.72
E_{VBM}		6.41	4.08	3.53	3.65	3.48
E_g		3.05	2.98	2.94	3.05	3.24
E_{\max}		3.05	1.88	2.39	3.05	2.61
m^*	CBM	0.35	0.38	0.40	0.42	0.46
	IL	—	5.43	1.21	—	2.73, 1.08
	VBM	0.92	1.28	0.95	1.30	1.25
						1.21

dopants and various doped models on the lattice constants and volume is very minor, within 0.74% and 1.37%, respectively. The reason may be that the atomic radius of the dopant is similar to that of the O atom. However, further observation from Fig. 1 found that dopants significantly affect the local structure and thus the electronic properties dramatically.

We have calculated the E_f to assess the stability of dopants into TiO₂, as shown in Table 1. All of them are positive (or negative) under O-rich (or Ti-rich) conditions. Negative E_f suggests that dopant tends to enter the TiO₂ lattice. Thus, this confirms that the N(F) atoms prefer to substitute the O atom under Ti-rich conditions, since more oxygen vacancies are present in this case.^{29,34} Meanwhile, the E_f of these doped systems have the relative relationships: $E_f(\text{N}_s\text{-F}_s) < E_f(\text{N}_i\text{-F}_s) < E_f(\text{N}_s\text{-F}_i) < E_f(\text{N}_s) < E_f(\text{N}_i\text{-F}_i)$ under Ti-rich conditions. Thus, N_s–F_s co-doped TiO₂ is the most stable system, due to its lowest

E_f (–6.92 eV). Moreover, the E_f of all co-doped TiO₂ (except for N_i–F_i co-doped TiO₂) is smaller than N doped TiO₂ indicates that the incorporation of the N atoms into the TiO₂ will be easier to achieve in the presence of the F dopant. Further, considering the relationship between E_f and μ_O , a variety of N/F co-doped TiO₂ can be synthesized by controlling the flow of O₂ and supplying enough energy.

3.2 Electronic properties

To demonstrate how doped atoms modify the electronic properties of TiO₂, the band structures and partial density of states (PDOS) of individual Ti, O, N and F atoms of all the systems are shown in Fig. 2 and 3, respectively. And the E_g , the Fermi level (E_F), the maximum energy gap in the band gap (E_{\max}), the energy of conduction band minimum (CBM) (E_{CBM}) and valence band maximum (VBM) (E_{VBM}) are listed in Table 1.

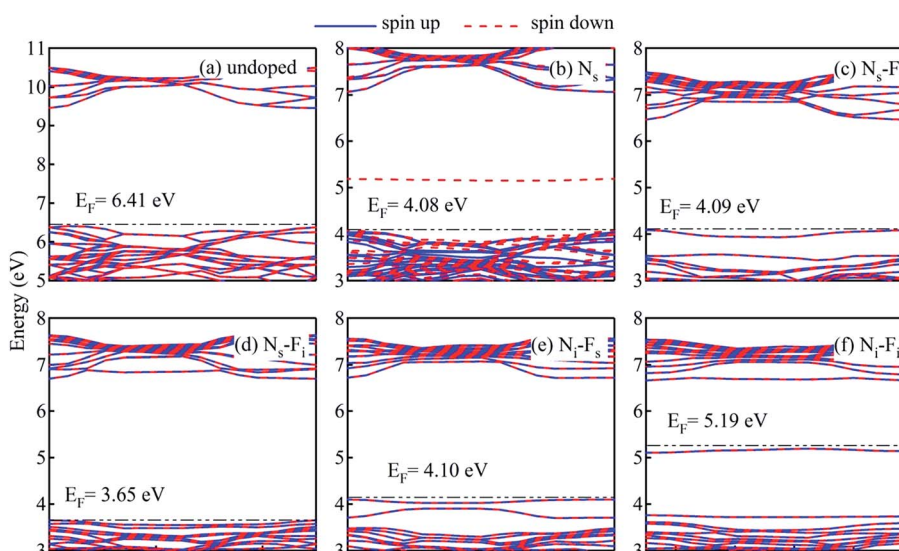


Fig. 2 The band structures of undoped and doped TiO₂, where the blue full (red dash) lines represent the spin up (spin down) states and the horizontal dashed lines denote the Fermi level (E_F).



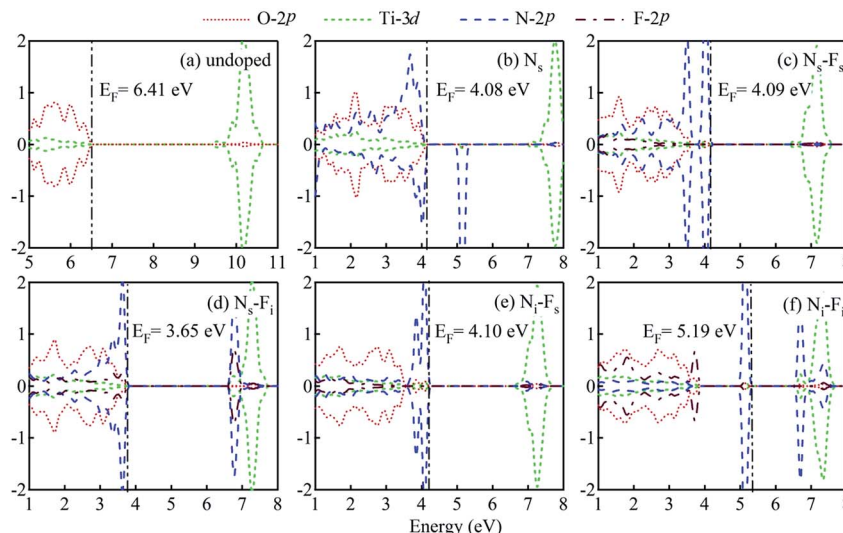


Fig. 3 PDOS of undoped and doped TiO_2 , the vertical dashed lines denote the Fermi level (E_F).

The band gap of TiO_2 is mostly controlled by O-2p and Ti-3d states, but the ILs of the dopants can also modify it. Thus the dopants can fine tune the band gap of the doped system. The details of the band gap tuning can be described as the followings.

For N_s doped TiO_2 (Fig. 2b and 3b), the valence band now has the half-filled N_s -2p state which is just above the original VBM, while the conduction band (CB) remain unchanged. Thus, the valence band (VB) lifts toward to the CB and the E_g is reduced by 0.07 eV. Similar to this, the filled IL of the N_s - F_s co-doped TiO_2 (Fig. 2c and 3c) is also above the VBM. Thus, the E_g is lowered to 2.94 eV compared to undoped TiO_2 . For the case of N_s - F_i co-doped TiO_2 (Fig. 2d and 3d) and N_i - F_i co-doped TiO_2 (Fig. 2f and 3f), the ILs overlap the original VB and CB, thus the band gap remains the same. For the case of N_i - F_s co-doped TiO_2 (Fig. 2e and 3e), the filled ILs locate in the middle of the band gap. And the VB is lowered due to missing one O atom. Thus the band gap increases compared to the undoped TiO_2 . This verifies that N and F atoms can modulate the electronic structure of the TiO_2 , by changing the position and amount of ILs. Furthermore, the spin polarization states present in the N_s doped TiO_2 is not observed in the co-doped system due to the charge compensation effect between N and F atom.

Overall, the doped system only reduces the band gap below 0.11 eV. In other words, the maximum red-shifted optical absorption edge is only 15.3 nm. However, the ILs in the band gap not only reduce the E_g , but also separate and promote photo-excited electrons pumping from the VB into the CB. These characteristics are likely to improve visible light photocatalytic activity. More details will be discussed later.

3.3 Effective mass of photogenerated carriers

We all know that the limited number of density of states and the low charge carrier mobility in the flat ILs limits its role as a stepping stones for electronic transition, and the electrons are easily annihilated by recombination with holes. The carrier mobility has been calculated according to the equation $\mu = e\tau/m^*$

m^* , where τ is the mean free time, m^* is the effective mass (both related to the curvature of the band level).^{40,41} Smaller efficient masses mean higher carrier mobility. The m^* of all the systems were presented in Table 1. The results show that there is a flat IL ($m^* = 5.43$) in the N_s doped TiO_2 that limits the separation of photogenerated carriers. In contrast, all co-doped systems have smaller m^* , especially N_s - F_s co-doped TiO_2 ($m^* = 1.21$). Thus, this IL suppresses the recombination rate. We believe that N_s - F_s co-doped TiO_2 will have the highest photocatalytic efficiency.

3.4 Band edge energy and photocatalytic properties

The band edges energy (E_{VBM} and E_{CBM}) determines the redox potential of the semiconductor photocatalyst. Fig. 4 and Table 1 indicate that the E_{VBM} and E_{CBM} of all doped TiO_2 move down to the low energy region (more than 2.33 eV), compared with the undoped TiO_2 . Such as, the oxidizability of photogenerated holes at the VBM is enhanced 2.33–2.93 eV, while the reducibility of photogenerated electrons at the CBM is reduced 2.40–

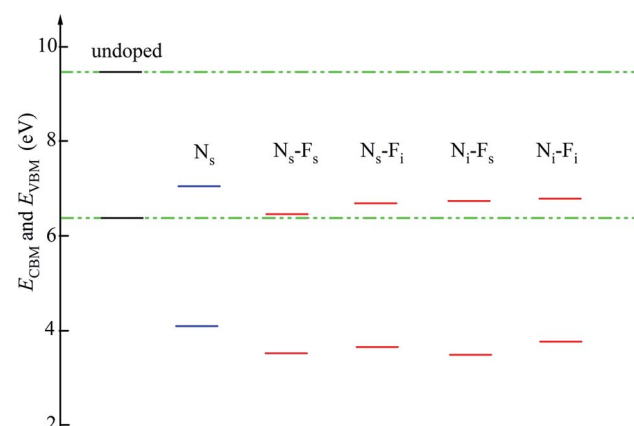


Fig. 4 The E_{CBM} and E_{VBM} of undoped (green dotted line) and doped (blue and red line) TiO_2 .



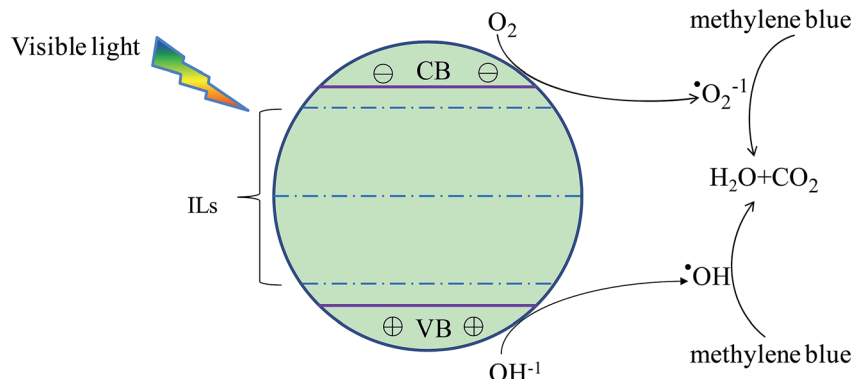


Fig. 5 The mechanism for photocatalytic degradation of MB by doped TiO_2 under visible light irradiation.

2.99 eV. Moreover, the band edges energy of N/F co-doped TiO_2 move more to the lower energy region compared with N_s doped TiO_2 . So, they have greater ability to modify the redox potentials; especially the N_s-F_s co-doped TiO_2 .

On the other hand, O_2^- ion and 'OH radical all are important oxidants in the process of photocatalytic degradation of methylene blue. The degradation mechanism is shown in Fig. 5. On the surface of TiO_2 , O_2^- ions are reduced by the photogenerated electrons from the O_2 , while 'OH radicals are oxidized by the photogenerated holes from the OH^- . Thus, all doped systems tend to produce more 'OH than O_2^- during the photocatalytic process. For that, as discussed above, we conclude that N_s-F_s co-doped model can explain the mechanism of enhanced photocatalytic activity in the recent experiments that the 'OH radical played a leading role during the visible light photocatalytic process.^{33,42-45} Meanwhile, volumes were 550.25 and 551.74 \AA^3 for N_s doped and N_s-F_s co-doped TiO_2 . This expanded surface area also promotes the photocatalytic ability of N_s-F_s co-doped TiO_2 .

4. Conclusions

In summary, the crystal structure, formation energy, electronic structures and effective masses of charge carriers of N doped and N/F co-doped TiO_2 were investigated by first-principles calculations. We have found that the Ti-rich growth condition is beneficial to all doped TiO_2 . Meanwhile, the incorporation of the N atom into the TiO_2 will be easier to achieve in the presence of the F dopant. N/F co-doped TiO_2 has no spin polarization, smaller effective mass and lower band edge energy. They, especially N_s-F_s co-doped TiO_2 , not only greatly improve the photogenerated carriers' mobility and separation, but also increase the oxidation ability of the photogenerated holes. Thus, we have explained the mechanism of the enhancement of photocatalytic efficiency of N/F co-doped TiO_2 observed by experiments. Moreover, this work also provides new insights into synthesis and design of the various-doped TiO_2 by controlling the flow of O₂ during sample preparation.

Conflicts of interest

There are no conflicts to declare.

Acknowledgements

This work is supported by the National Key Research and Development Program of China (No. 2016YFA0300803), the National Basic Research Program of China (No. 2014CB921101), the National Natural Science Foundation of China (No. 61474061, 61674079), Jiangsu Shuangchuang Program and the Natural Science Foundation of Jiangsu Province of China (No. BK20140054). Computational resources were provided by the Jilin University.

References

- 1 A. L. Linsebigler, G. Lu and J. T. Yates, *Chem. Rev.*, 1995, **95**, 735.
- 2 M. R. Hoffmann, S. T. Martin, C. Wonyong and D. W. Bahnemann, *Chem. Rev.*, 1995, **95**, 69.
- 3 I. Nakamura, S. Kutsuna, T. Ihara, S. Sugihara and K. Takeuchi, *J. Mol. Catal. A: Chem.*, 2000, **161**, 205.
- 4 Y. Q. Wang, R. R. Zhang, J. B. Li, L. L. Li and S. W. Lin, *Nanoscale Res. Lett.*, 2014, **9**, 46.
- 5 X. P. Cao, D. Li, W. H. Jing, W. H. Xing and Y. Q. Fan, *J. Mater. Chem.*, 2012, **22**, 15309.
- 6 S. U. M. Khan, M. A. Shahry and W. B. Ingler Jr, *Science*, 2002, **297**, 2243.
- 7 H. Wang and J. P. Lewis, *J. Phys.: Condens. Matter*, 2006, **18**, 421.
- 8 C. Li, Y. F. Zhao, Y. Y. Gong, T. Wang and C. Q. Sun, *Phys. Chem. Chem. Phys.*, 2014, **16**, 21446.
- 9 C. D. Valentin and G. Pacchioni, *Catal. Today*, 2013, **206**, 12.
- 10 Y. F. Zhao, C. Li, J. Y. Hu, Y. Y. Gong, L. Y. Niu and X. J. Liu, *Phys. Lett. A*, 2016, **380**, 910.
- 11 J. Q. Wen, X. Li, W. Liu, Y. P. Fang, J. Xie and Y. H. Xu, *Chin. J. Catal.*, 2015, **36**, 2049.
- 12 W. L. Yu, J. F. Zhang and T. Y. Peng, *Appl. Catal., B*, 2016, **181**, 220.
- 13 Y. F. Zhao, C. Li, S. Lu and L. J. Yan, *Chem. Phys. Lett.*, 2016, **647**, 36.
- 14 J. G. Yu, P. Zhou and Q. Li, *Phys. Chem. Chem. Phys.*, 2013, **15**, 12040.



15 C. D. Valentin, E. Finazzi, G. Pacchioni, A. Selloni, S. Livraghi, M. C. Paganini and E. Giamello, *Chem. Phys.*, 2007, **338**, 44.

16 C. Y. Jimmy, J. G. Yu, W. Ho, Z. T. Jiang and L. Z. Zhang, *Chem. Mater.*, 2002, **14**(9), 3808.

17 J. Xu, B. F. Yang, M. Wu, Z. P. Fu, Y. Lv and Y. X. Zhao, *J. Phys. Chem. C*, 2010, **114**, 15251.

18 Y. Y. Wu, Y. M. Ding, X. F. Xia, X. Liu and H. X. Li, *Appl. Surf. Sci.*, 2016, **364**, 829.

19 M. S. Akple, J. X. Low, Z. Y. Qin, S. Wageh, A. A. Al-Ghamdi, J. G. Yu and S. W. Liu, *Chin. J. Catal.*, 2015, **36**, 2127.

20 J. Georgieva, E. Valova, S. Artyanov, D. Tatchev, S. Sotiropoulos, I. Avramova, N. Dimitrova, A. Hubin and O. Steenhaut, *Appl. Surf. Sci.*, 2017, **413**, 284.

21 J. S. Zhou, F. Z. Li, C. Du, J. M. Liu, Y. Z. Wang, W. Li, G. N. He and Q. Y. He, *RSC Adv.*, 2016, **6**, 84457.

22 L. Hao, Z. W. Wang, Y. Q. Zheng, Q. Q. Li, S. J. Guan, Q. Zhao, L. J. Cheng, Y. Lu and J. Z. Liu, *Appl. Surf. Sci.*, 2017, **391**, 275.

23 P. Zhou, J. H. Wu, W. L. Yu, G. H. Zhao, G. J. Fang and S. W. Cao, *Appl. Surf. Sci.*, 2014, **319**, 167.

24 K. Shen, X. Xue, X. Y. Wang, X. Y. Hu, H. W. Tian and W. Zheng, *RSC Adv.*, 2017, **7**, 23319.

25 P. Zhou, J. G. Yu and Y. X. Wang, *Appl. Catal., B*, 2013, **45**, 142.

26 C. D. Valentin, E. Finazzi and G. Pacchioni, *Chem. Mater.*, 2008, **20**, 3706.

27 B. P. Dhamanir, A. Kumar, A. K. Srivastava and J. S. Tawale, *Res. Chem. Intermed.*, 2017, **43**, 387.

28 J. W. J. Hamilton, J. A. Byrne, P. S. M. Dunlop, D. D. Dionysiou, M. Pelaez, K. O'Shea, D. Synnott and S. C. Pillai, *J. Phys. Chem. C*, 2014, **118**, 12206.

29 S. H. Shin, H. H. Chun and W. K. Jo, *Materials*, 2015, **8**, 31.

30 J. Y. Cheng, J. Chen, W. Lin, Y. D. Liu and Y. Kong, *Appl. Surf. Sci.*, 2015, **332**, 573.

31 J. P. Perdew, K. Burke and M. Ernzerhof, *Phys. Rev. Lett.*, 1996, **77**, 3865.

32 D. R. Hamann, M. Schluter and C. Chiang, *Phys. Rev. Lett.*, 1979, **43**, 1494.

33 Y. Lv, Z. P. Fu, B. F. Yang, J. Xu, M. Wu, C. Q. Zhu and Y. X. Zhao, *Mater. Res. Bull.*, 2011, **46**, 361.

34 N. Janpatch, C. Vanichvattanadecha and R. Rujiravanit, *Cellulose*, 2015, **22**, 3321.

35 C. Li, J. C. Li, J. S. Lian and Q. Jiang, *J. Appl. Phys.*, 2009, **106**, 094102.

36 M. E. Arroyo-de Dompablo, A. M. Garcia and M. Taravillo, *J. Chem. Phys.*, 2011, **135**, 054503.

37 P. Deak, B. Aradi and T. Frauenheim, *Phys. Rev. B: Condens. Matter Mater. Phys.*, 2011, **83**, 155207.

38 <http://www.webelements.com>.

39 M. Horn, C. F. Schwerdtfeger and E. P. Meagher, *Z. Kristallogr.*, 1972, **136**, 273.

40 A. R. West, *Basic Solid State Chemistry*, John. Wiley, Chichester, 1999, p. 49.

41 T. H. Wang, Y. F. Zhou and Q. Jiang, *J. Phys. Chem. C*, 2013, **117**, 12873.

42 Q. Guo, Z. H. Zhang, X. P. Ma, K. Jing, M. L. Shen, N. Yu, J. H. Tang and D. D. Dionysiou, *Sep. Purif. Technol.*, 2017, **175**, 305.

43 A. E. Giannakas, E. Seristatidou, Y. Deligiannakis and I. Konstantinou, *Appl. Catal., B*, 2013, **132**, 460.

44 A. V. Katsanaki, A. G. Kontos, T. Maggos and M. Pelaez, *Appl. Catal., B*, 2013, **140**, 619.

45 D. Li, N. Ohashi, S. Hishita, T. Kolodiaznyi and H. Haneda, *J. Solid State Chem.*, 2005, **178**, 3293.